In vivo severity ranking of Ras pathway mutations associated with developmental disorders

Granton A. Jindal[a,b,c,1], Yogesh Goyal[a,b,1], Kei Yamaya[b,c], Alan S. Futran[a,b], Iason Kountouridis[b], Courtney A. Balgobin[c], Trudi Schüpbach[c], Rebecca D. Burdine[c], and Stanislav Y. Shvartsman[a,b,c,2]

[a]Department of Chemical and Biological Engineering, Princeton University, Princeton, NJ 08544; [b]Lewis-Sigler Institute for Integrative Genomics, Princeton University, Princeton, NJ 08544; and [c]Department of Molecular Biology, Princeton University, Princeton, NJ 08544

Edited by Denis Duboule, University of Geneva, Geneva, Switzerland, and approved December 1, 2016 (received for review September 19, 2016)

Germ-line mutations in components of the Ras/MAPK pathway result in developmental disorders called RASopathies, affecting about 1/1,000 human births. Rapid advances in genome sequencing make it possible to identify multiple disease-related mutations, but there is currently no systematic framework for translating this information into patient-specific predictions of disease progression. As a first step toward addressing this issue, we developed a quantitative, inexpensive, and rapid framework that relies on the early zebrafish embryo to assess mutational effects on a common scale. Using this assay, we assessed 16 mutations reported in MEK1, a MAPK kinase, and provide a robust ranking of these mutations. We find that mutations found in cancer are more severe than those found in both RASopathies and cancer, which, in turn, are generally more severe than those found only in RASopathies. Moreover, this rank is conserved in other zebrafish embryonic assays and *Drosophila*-specific embryonic and adult assays, suggesting that our ranking reflects the intrinsic property of the mutant molecule. Furthermore, this rank is predictive of the drug dose needed to correct the defects. This assay can be readily used to test the strengths of existing and newly found mutations in MEK1 and other pathway components, providing the first step in the development of rational guidelines for patient-specific diagnostics and treatment of RASopathies.

MEK1 | zebrafish | *Drosophila* | RASopathies | MEK inhibitor

The Ras/MAPK (rat sarcoma/mitogen-activated protein kinase) signaling pathway is involved in essentially all aspects of organismal development, from the first cell divisions in the early embryo to postnatal development and growth (1–3). Given its critical function, it is not surprising that deregulated Ras/MAPK signaling, resulting from either genetic or environmental perturbations, can lead to developmental abnormalities. A large class of such abnormalities, known as RASopathies, is associated with activating germ-line mutations in many components of the Ras pathway (4). Estimated to affect 1/1,000 human births, these abnormalities are characterized by a broad spectrum of phenotypes, including cardiac defects, craniofacial dysmorphisms, and neurocognitive delays (4). Although the origins of these phenotypes are still poorly understood, studies of model organisms show that many of the observed structural and functional defects can indeed be mimicked by targeted introduction of mutations found in RASopathies (5). Hundreds of such mutations have already been identified, and many more are likely to be discovered by the sequencing of affected individuals (6).

Importantly, these studies identify new mutations in the very same components that are mutated in cancer and have been extensively studied both in vitro and in vivo (7–9). In particular, multiple new mutations were identified in MEK1, a MAPK kinase (10) and an important target for anticancer therapeutics (11–19). Because it is commonly believed that cancer mutations would be embryonic lethal when inherited through the germ line, it might be expected that mutations that cause developmental disorders, but allow survival of the carrier, are weaker than those that cause cancer (20). However, some of the MEK1 RASopathy mutations have also been recently reported in cancer (21, 22), challenging to some extent the notion that cancer mutations are more severe than RASopathy mutations. Currently, most phenotypic analyses in RASopathies are based on comparison at the gene level (23–26), but there is high phenotypic heterogeneity within patients having mutations in the same gene (12). Independent of genetic background, it is important to know whether some mutations can cause more severe phenotypes than others. The answers to this and related questions may provide rational guidelines for predicting disease progression and suggest strategies for their management and therapeutic treatment of affected individuals.

Although previous studies have indirectly observed mutation-based severity of effects using cultured cells (16, 27, 28) and model organisms (29–31) by comparing a few mutations, in no case were the studies comprehensive. To address this more systematically, we develop a framework for the quantitative comparison of MEK1 mutants found in human diseases. Our approach relies on quantitative analysis of morphological effects caused by these activating mutations in zebrafish (*Danio rerio*) and fruit flies (*Drosophila melanogaster*). First, using experiments in the early zebrafish embryo, we discover a clear ranking of mutations. Specifically, mutations found in cancer were more severe than those found in both RASopathies and cancer, which, in turn, were generally more severe than those found only in RASopathies. Furthermore, we develop a quantitative assay to measure heart size of a developing zebrafish embryo and find that the ranking is preserved in this assay. Importantly, this ranking is largely consistent with the relative effects of the same mutations in *Drosophila*. This shows that our assays reveal the intrinsic property of affected molecules and not the property of the model organism in which these mutations are tested. Furthermore, we find that the established ranking can be used to predict, for different mutations, the dose of pharmacological MEK inhibitors, which have been proposed as a potential strategy for correcting these developmental defects

Significance

RASopathies are developmental disorders caused by germ-line mutations in Ras/MAPK pathway components. Hundreds of such mutations have been reported using patient-specific sequencing projects. However, a systematic framework to translate individual mutations into patient-specific phenotypic severity is missing. Here, we develop such a framework by focusing on mutations in MEK1, a MAPK kinase. We report that the aspect ratio of early zebrafish embryos can be used as a metric to efficiently rank these mutations. Furthermore, this rank is conserved in other zebrafish- and *Drosophila*-specific assays and is predictive of drug dose needed to reverse the aspect ratio. Our results suggest that a systematic mutation-based comparative analysis of human phenotypes is crucial for efficient diagnosis and potential treatment.

Author contributions: G.A.J., Y.G., T.S., R.D.B., and S.Y.S. designed research; G.A.J., Y.G., K.Y., I.K., and C.A.B. performed research; A.S.F. contributed new reagents/analytic tools; G.A.J., Y.G., and K.Y. analyzed data; and G.A.J., Y.G., T.S., R.D.B., and S.Y.S. wrote the paper.

The authors declare no conflict of interest.

This article is a PNAS Direct Submission.

[1]G.A.J. and Y.G. contributed equally to this work.

[2]To whom correspondence should be addressed. Email: stas@princeton.edu.

This article contains supporting information online at www.pnas.org/lookup/suppl/doi:10.1073/pnas.1615651114/-/DCSupplemental.

(32). The established ranking and the experimental approaches provide a natural framework for evaluating the biological effects of not only already identified mutations but also yet-to-be-discovered sequence variants of MEK1 and other components of the Ras/MAPK pathway.

Results

Ranking of MEK1 RASopathy Mutations in Zebrafish. Ectopic Ras/MAPK signaling in the early zebrafish embryo has been reported to cause dorsalization, which is apparent through pleiotropic phenotypes, including oval shape of the embryo at 11 h post-fertilization (hpf), which is caused by abnormal convergence and extension movements during gastrulation (33, 34). This easily detectable oval shape phenotype in the zebrafish embryo was first noticed to be caused by RASopathy variants in Shp2, a protein tyrosine phosphatase (35), and later observed with four MEK1 RASopathy mutations (36). This assay has since been used in a more quantitative manner by using the major-to-minor axis ratio of the zebrafish embryo as a metric to denote the severity of the defect (29). Because previous studies measured embryo shapes at different times, we measured the major-to-minor axis ratio (aspect ratio) over time and determined 11 hpf as the best time to maximize dynamic range (*SI Appendix*, Figs. S1 and S2*A*), a time point where we see minimal lethality that would render the embryos unscorable. Measuring the ratio at 11 hpf for both wild-type (WT) and injected embryos yields distributions that can be used to quantitatively characterize the severity of defect (*SI Appendix*, Fig. S2*B*).

We synthesized mRNA for WT MEK1; 14 reported RASopathy MEK1 variants (11–18), of which 5 are also found in cancer (37); and two MEK1 variants that are found in cancer alone (37) (Fig. 1*A* and *SI Appendix*, Table S1). By injecting an equal amount of mRNA into all zebrafish embryos, we induced expression of similar amounts of MEK1 protein (*SI Appendix*, Fig. S3) and found that MEK1 mutations result in varying degrees of aspect ratio at 11 hpf. Specifically, we found a clustering of three classes of mutations, such that those found only in cancer had the highest ratio, followed by those found in both cancer and RASopathies, whereas those found in RASopathies alone had the lowest ratios (Fig. 1*B* and *SI Appendix*, Table S2). There were a few exceptions to this categorization, namely F53S and Y130H, which are found to be at least as severe as mutations found in both RASopathies and cancer. Based on this observation, we predict that there is a possibility that these mutations might be found in cancer in the future. Conversely, some currently cancer-only mutations may lie in the RASopathies and cancer region and may be found to cause RASopathies in the future. Because Ras/MAPK signaling is involved in many developmental processes, we also determined the amount of embryonic lethality at 48 hpf. The clustering observed in our ranking by aspect ratio is largely consistent with the fraction of embryos that die, although the lethality assay is not as differentiating between mutations (Fig. 1*C* and *SI Appendix*, Table S3).

Heart defects, including hypertrophic cardiomyopathy, which is marked by increased heart size, are clinical phenotypes observed in cardio-facio-cutaneous syndrome, a RASopathy (38). Previous studies reported that RASopathy mutations in Shp2 do not affect heart size at 20 hpf based on *myl7* in situ hybridizations, although left–right asymmetry is affected at a later time (39). Other studies using pharmacological activation of the Ras/MAPK pathway, however, have shown an increase in heart size at 18 hpf using *myl7* in situ hybridizations (40). To reconcile these opposing findings, we developed a quantitative assay using two-photon microscopy to capture the size of the primordia in a line of zebrafish with green fluorescent protein (GFP) under the control of the *myl7* promoter (Fig. 2*A*). We characterized the surface area of the maximum intensity projection at 19.5 hpf of hearts from fixed embryos injected with a MEK1 variant and hearts from their uninjected siblings (Fig. 2*B*). We performed this analysis for mutations in each of the three classes and normalized the heart size of the embryos injected with a MEK1 variant by the average of that of their uninjected siblings. We found that zebrafish carrying more

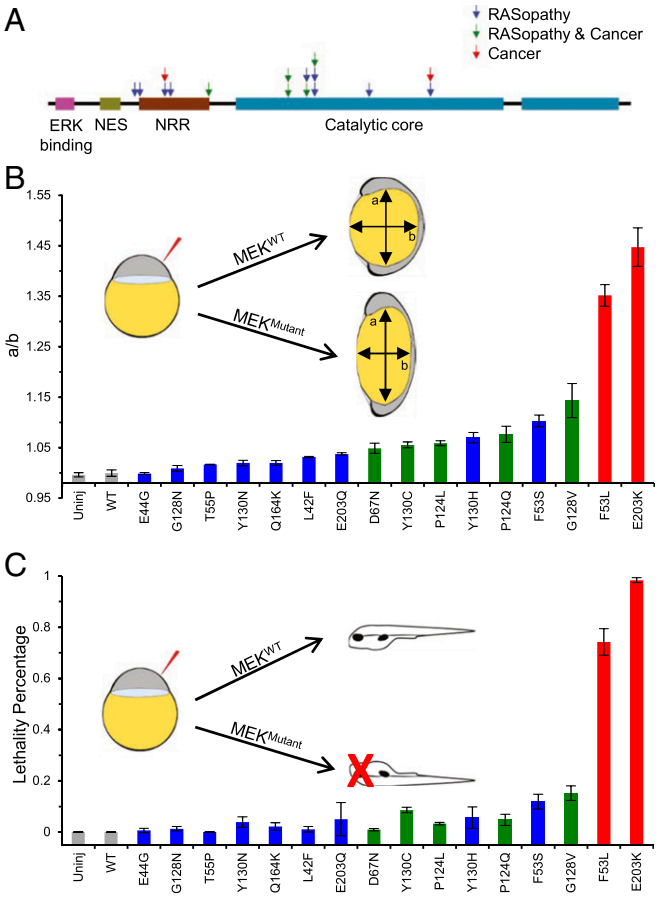

Fig. 1. Ranking of MEK1 RASopathy mutations in zebrafish. (*A*) Schematic representation of the MEK1 protein with mutations that cause RASopathies (blue), RASopathies as well as cancer (green), and cancer only (red). (*B*) Rank of 16 activating MEK mutations based on the oval shape of the zebrafish embryo at 11 hpf upon injection of MEK mRNA with an activating mutation. The oval shape was quantified as the ratio of the major (a) to minor (b) axis (see *Inset*) or a/b. The average of at least three technical replicates for each mutation is plotted with the SEM indicated (for *N* values and *P* values of pairwise comparisons, see *SI Appendix*, Table S2)—each technical replicate being the average of about 30 embryos. (*C*) Embryonic lethality at 48 hpf after injection of MEK mRNA with an activating mutation. The average of at least three technical replicates for each mutation is plotted with the SEM indicated (for *N* values and *P* values of pairwise comparisons, see *SI Appendix*, Table S3). The Kruskal–Wallis test with the Bonferroni correction was used for statistical analysis.

severe MEK1 mutations had larger hearts, yielding a ranking that is consistent with the aspect ratio assay (Fig. 2*C*). Note that a difference between the zebrafish MEK1 models and human hypertrophic cardiomyopathy is that the enlarged zebrafish heart has more cells than normal, but of similar size, whereas enlarged human hearts have similar numbers of cells with larger size than normal (38, 40).

In summary, we have developed a rigorous, inexpensive, and rapid framework to rank mutations by strength. Furthermore, we have shown that our ranking is consistent with assays of embryonic lethality and heart size in zebrafish.

Ranking of MEK1 RASopathy Mutations in *Drosophila*. The general question for any assay, such as expression of MEK1 in the early zebrafish embryo, is the extent to which the results reflect the true property of the tested molecule versus a property of the system into which it is introduced. To address this question, we examined the effects of a select group of mutations in the fruit fly. We expressed Dsor1, the fly ortholog of MEK, during early embryogenesis by using a maternal driver (MTD-Gal4). The mutation positions used in this section reflect the corresponding positions in human MEK1.

DEVELOPMENTAL BIOLOGY

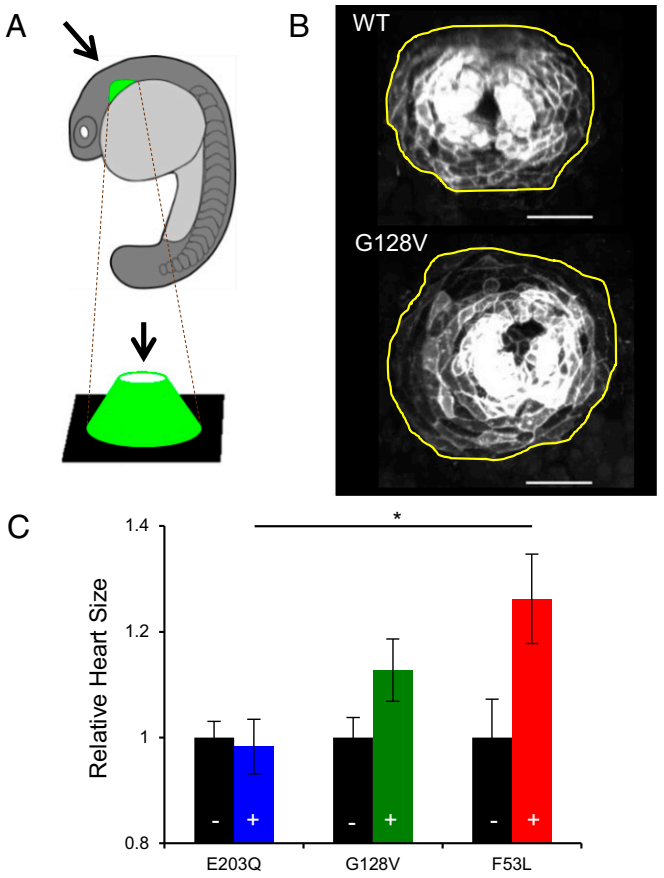

Fig. 2. Ranking of MEK1 RASopathy mutations in the zebrafish heart. (*A*) Schematic of zebrafish orientation during heart imaging. (*B*) Representative images of the zebrafish heart at 19.5 hpf with the outline of the heart in yellow. Cardiac cells are labeled by membrane GFP expressed from the *myl7* promoter. (Scale bar, 50 μm.) (*C*) Rank of selected mutations based on zebrafish heart size in embryos overexpressing MEK variants (+) compared with uninjected siblings (–, black). The average for each mutation is plotted with the SEM indicated. RASopathies, blue; RASopathies and cancer, green; cancer only, red. Here, *N* values are $N_{E203Q,-} = 12$, $N_{E203Q,+} = 9$, $N_{G128V,-} = 12$, $N_{G128V,+} = 9$, $N_{F53L,-} = 9$, and $N_{F53L,+} = 8$. One-way analysis of variance (ANOVA) with Bonferroni correction was used for statistical analysis: $*P < 0.1$. The differences of the following pairs were not statistically significant: E203Q, G128V; G128V, F53L.

Furthermore, for the mutations we used for characterization, the amino acids were conserved in all but one case, where at residue 44, instead of glutamic acid (E), there was a structurally similar aspartic acid (D). Although expression of WT Dsor1 did not produce phenotypes, we observed defects in larval cuticles including segmentation defects, minor defects in head structures, and occasional holes in the cuticular midbody when we expressed Dsor1-carrying RASopathy mutations (Fig. 3*A*). Furthermore, we found that the eight larval abdominal segments, characterized by anterior denticle belts in WT, are reduced to about five (*SI Appendix*, Fig. S4). These phenotypes are similar to those reported for different gain-of-function (GOF) mutations in Torso, a receptor tyrosine kinase (RTK) (41). These defects result in embryonic lethality, albeit to various degrees for different mutants (Fig. 3*B*). For example, although overexpression of WT and D44G versions of Dsor1 lead to no significant lethality, overexpression of other mutants resulted in high lethality (Fig. 3*B*). However, the assay could not differentiate between F53S, F53L, and E203K, suggesting that the fly lethality assay is at saturation for highly activating mutations and that other assays should be used to compare highly activating mutations. Nevertheless, the mutation-specific severity is broadly conserved from zebrafish- to fly-specific embryonic assays.

To study whether such a rank is preserved during adulthood, we used a Tubulin-Gal4 driver to ubiquitously drive expression of Dsor1 variants. Ras/MAPK signaling is involved in wing formation, and we quantified the defects induced by GOF mutations, which include formation of stereotypic ectopic veins (31, 42). Surprisingly, D44G, which does not show any significant deviation from WT in zebrafish and fly embryonic assays, displayed ectopic wing veins, suggesting either that this mutation displays more activity in this context or that wing development is more sensitive to pathway perturbations (Fig. 4*A*). In addition, we could consistently rank the other mutations, and E203K was the most severe mutation, consistent with the aspect ratio assay (Fig. 4 *B* and *C*). Furthermore, the severity of wing defects was sex-specific, such that wings of females had more defects, although the respective ranking was conserved (Fig. 4 *B* and *C*). This is also consistent with a recent report that fly wings display sex-dependent effects in different genetic backgrounds (43). Additionally, multiple studies have suggested a role of sex on the severity of defects in individuals with RASopathies. For example, studies of RASopathy mouse models associated with Neurofibromatosis 1 (NF1) showed that females have more severe neuronal dysfunction than males (44).

These findings indicate that the severity of effects of mutations from embryonic and adult assays in *Drosophila* is consistent with those found in fish. Furthermore, these results from the fly suggest that some assays are more sensitive to weak genetic perturbations

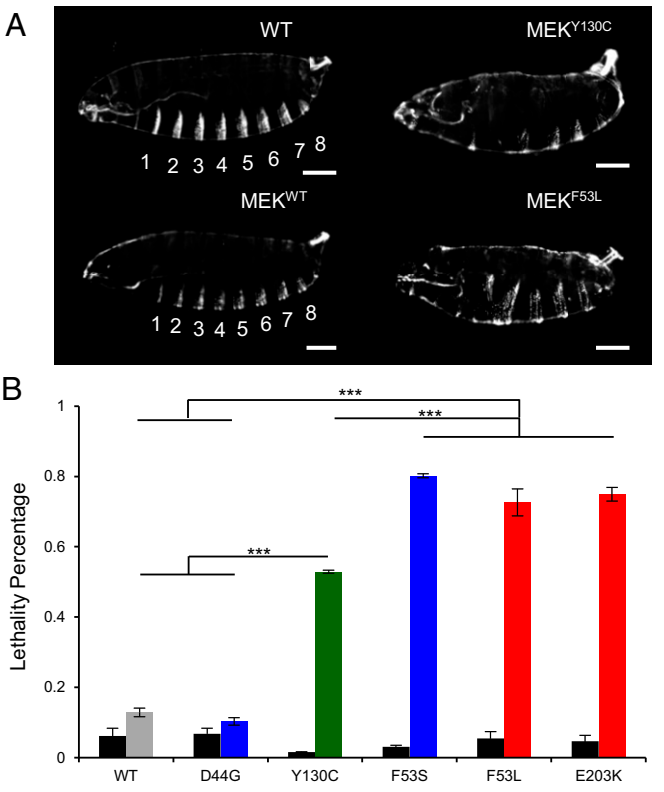

Fig. 3. Ranking of MEK1 RASopathy mutations in *Drosophila*. (*A*) Larval cuticle defects in flies with overexpressed MEK variants using MTD-Gal4. (Scale bar, 100 μm.) (*B*) Rank of selected MEK mutations based on embryonic lethality. The average of technical replicates for each mutation is plotted with the SEM indicated. RASopathies, blue; RASopathies and cancer, green; cancer only, red. Here, pooled *N* values are as follows: $N_{WT} = 286$, $N_{D44G} = 282$, $N_{Y130C} = 382$, $N_{F53S} = 382$, $N_{F53L} = 873$, and $N_{E203K} = 907$. Black bars represent basal lethality in the UAS-MEK-WT/Mutant transgenic flies without the presence of a Gal4 driver. Here, $N_{WT} = 502$, $N_{D44G} = 279$, $N_{Y130C} = 277$, $N_{F53S} = 265$, $N_{F53L} = 317$, and $N_{E203K} = 287$. One-way analysis of variance (ANOVA) with Bonferroni correction was used for statistical analysis: $***P < 0.001$. The differences of the following pairs were not statistically significant: WT, D44G; F53S, F53L; F53S, E203K; F53L, E203K.

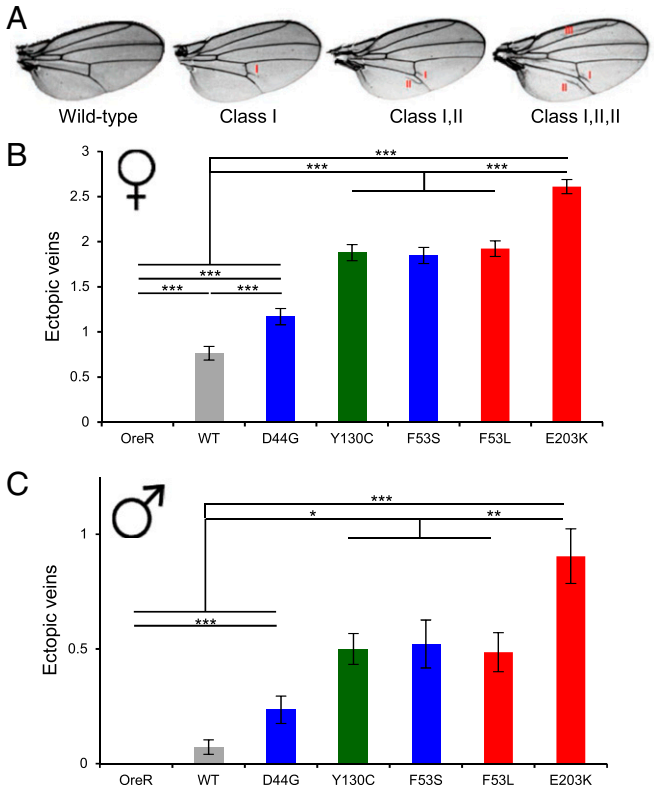

Fig. 4. Ranking of MEK1 RASopathy mutations in the *Drosophila* wing. (*A*) Ectopic wing veins in flies with overexpressed MEK variants using a low-level ubiquitous driver (Tub-Gal4). Here, classes denote ectopic wing veins at specific locations in the wing. (*B* and *C*) Rank of selected MEK mutations based on the number of ectopic wing veins from all classes in females (f) and males (m). The average for each mutation is plotted with the SEM indicated. RASopathies, blue; RASopathies and cancer, green; cancer only, red. Here, $N_{OreR,m} = 404$, $N_{OreR,f} = 335$, $N_{WT,m} = 69$, $N_{WT,f} = 59$, $N_{D44G,m} = 68$, $N_{D44G,f} = 71$, $N_{Y130C,m} = 70$, $N_{Y130C,f} = 66$, $N_{F53S,m} = 23$, $N_{F53S,f} = 85$, $N_{F53L,m} = 70$, $N_{F53L,f} = 77$, $N_{E203K,m} = 42$, and $N_{E203K,f} = 59$. One-way analysis of variance (ANOVA) with Bonferroni correction was used for statistical analysis: $*P < 0.1$, $**P < 0.01$, $***P < 0.001$. The differences of the following pairs were not statistically significant: (*B*) Y130C, F53S; Y130C, F53L; F53S, F53L; (*C*) OreR, WT; WT, D44G; Y130C, F53S; Y130C, F53L; F53S, F53L.

than others. The consistency of our zebrafish and fly results suggests that we can reliably use the aspect ratio assay to carry out comparative analysis of mutations on a common quantitative scale.

Quantitative Effects of Drug Dose on Reversal of Phenotypes. Clinical phenotypes of RASopathies include both embryonic and postnatal defects, the latter of which might be partially reversible in humans pharmacologically (4). Previous studies have attempted to pharmacologically reverse prenatal defects in mice that have in utero fertilized embryos (45) and embryonic defects in zebrafish that have ex utero fertilized embryos (36, 46). Specifically, Ras/MAPK pathway inhibitors were used to correct the developmental abnormalities induced by RASopathies in zebrafish. Experiments in zebrafish have revealed that a 1-μM dose of MEK inhibitor from 4.5 to 5.5 hpf reverses early embryonic defects and lethality for different MEK mutations (36). However, it is unclear whether there is a minimum dose sufficient to reverse certain defects while still low enough to ensure that there are no deleterious side effects. Furthermore, if our rank is predictive, one might expect that mutations scoring weaker with our assay would need a smaller dose of pharmacological inhibitor. Here, we choose a mutation from each of the three classes to determine the minimal dose of drug that reverses the phenotype.

To test this hypothesis, we administered PD0325901, a second-generation MEK inhibitor, at various concentrations for a specific time window (Fig. 5*A*). We found that the minimal concentration that rescues the aspect ratio was consistent with the rank revealed by the aspect ratio assay (Fig. 5*B* and *SI Appendix*, Table S4). For example, although embryos carrying G128V required 1 μM of PD0325901, F53L required a 10-fold higher concentration (10 μM), whereas E203Q needed only 0.5 μM to reverse the defect, suggesting the need for patient-specific drug doses. Hence, here we show that RASopathy mutations have different reversal drug concentrations.

The combined effects of aberrant MAPK signaling on different cell types may result in embryonic lethality because Ras/MAPK signaling is involved in multiple processes during zebrafish development. Therefore, we also studied the rescue of

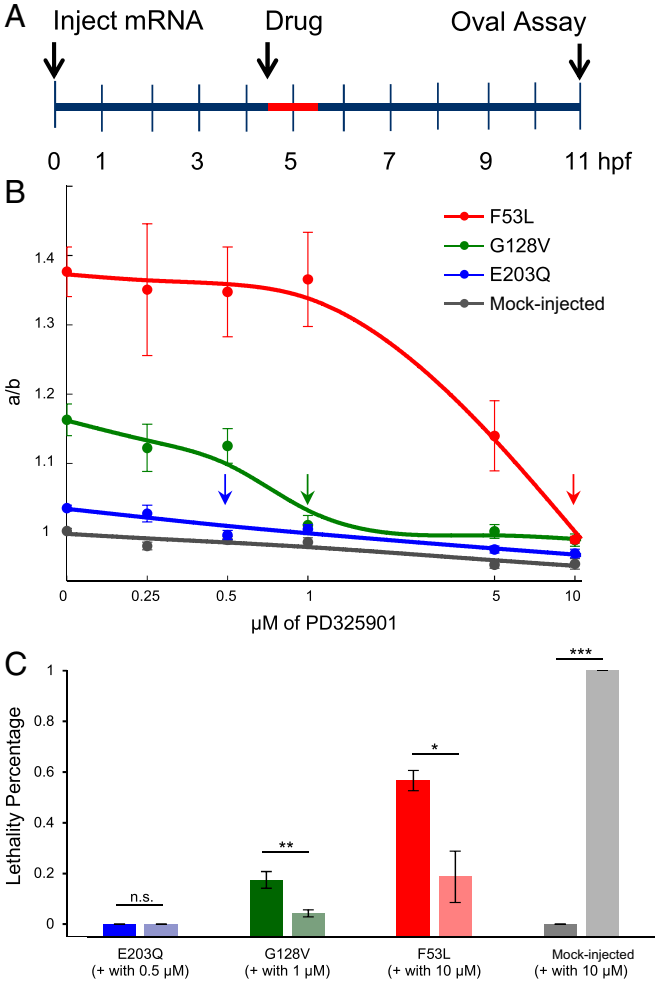

Fig. 5. Quantitative effects of drug dose on reversal of phenotype. (*A*) Schematic of drug treatment assay where mRNA is injected at 0 hpf, embryos were subjected to drug treatment from 4.5 to 5.5 hpf (red), and embryo shapes were measured at 11 hpf. (*B*) Reversal of oval embryo phenotype with varying doses of MEK inhibitor for F53L (red), G128V (green), E203Q (blue), and mock-injected (gray). The average for each mutation at the drug dose tested is plotted with the SEM indicated (for *N* values and *P* values of pairwise comparisons, see *SI Appendix*, Table S4). One-way analysis of variance (ANOVA) with Bonferroni correction was used for statistical analysis. Arrows indicate reversal doses of MEK inhibitor for each mutation. (*C*) Embryonic lethality measured with and without the reversal dose of MEK inhibitor for E203Q (blue), G128V (green), F53L (red), and mock-injected (gray). The average of at least three technical replicates for each mutation is plotted with the SEM indicated. Student's *t* test (two-sided, homoscedastic) was used for statistical analysis: not significant (n.s.), $*P < 0.1$, $**P < 0.01$, $***P < 0.001$. Here, pooled *N* values are as follows (–, without drug; +, with drug): $N_{E203Q,-} = 39$, $N_{E203Q,+} = 59$, $N_{G128V,-} = 57$, $N_{G128V,+} = 70$, $N_{F53L,-} = 55$, $N_{F53L,+} = 58$, $N_{Mock,-} = 18$, and $N_{Mock,+} = 53$.

lethality using the drug concentrations that were sufficient to correct oval embryo shape as determined above. As expected, the MEK inhibitor reduced the embryonic lethality for the G128V and F53L MEK1 variants (Fig. 5*C*). However, even very high doses of MEK inhibitor (10 μM) could not fully rescue the lethality for F53L (Fig. 5*C*). Furthermore, upon treating mock-injected WT embryos with the dose used for correcting F53L (10 μM), 100% of the embryos die, as characterized by a malformed tail (Fig. 5*C*). This could be a result of embryo elongation along the minor axis b (i.e., aspect ratio < 1) observed with 10 μM (Fig. 5*B*). Therefore, the dose for each mutation should not be too high or else the deleterious side effects may become overwhelming. To summarize, because the minimum dose for each mutation differs significantly, it is not appropriate to apply a common dose to all of the different RASopathy mutations.

Discussion

As sequencing becomes cheaper and more readily available, there is now an increased emphasis on developing patient-specific diagnoses and treatments. There is an increasing realization that many human diseases are dependent on the unique single nucleotide polymorphisms (SNPs) that exist in an individual. As an example, cancer treatments and therapeutics are beginning to be designed around the concept of personalized medicine (47). Because hundreds of mutations have already been reported to be associated with RASopathies, we believe that the disease prognosis should take into account information about the specific SNPs associated with the disease.

To perform a comparative analysis of mutations, we chose an appropriate assay by comparing the specific strengths and weaknesses of existing assays. For example, a simple approach using purified components in a test tube and quantifying kinase activity does not necessarily provide an accurate measure of functional implications in vivo. Another approach, comparing mutational strengths in cultured cell assays, yields a cellular context, but it is usually difficult to provide a mixture of endogenous growth factors that precisely mimic normal cellular environments. These assays also do not allow monitoring of development in time and 3D space, making it therefore difficult to predict the consequences of specific mutations on crucial features of a developing organism. Finally, it would be very time-intensive to create the ideal disease model of transgenic mice with the RASopathy mutations knocked into the endogenous locus and then perform a comparative developmental analysis. Here, we decided instead to use mRNA microinjection into zebrafish, and this provided us with an excellent functional assay for assessing mutation strength. The aspect ratio assay not only is quick but also takes place in a developing organism with organ structure and physiological levels of growth factors. Indeed, using this controlled experimental framework, we were able to show that activating mutations in MEK1 have different strengths. Furthermore, we found this assay to be more informative than the activated MAPK Western blot assay on zebrafish embryos, which could not differentiate between mutations as reliably (*SI Appendix*, Fig. S5).

A notable feature of RASopathies is that they affect only a subset of organs and to varying degrees. Although we see a consistent ranking of mutations in developing flies and zebrafish, we find that the sensitivity in terms of measurable phenotypes can be different in various cellular contexts (*SI Appendix*, Fig. S6). In flies, for example, we find an aberrant larval cuticle phenotype and ectopic wing veins, both of which are Ras/MAPK-dependent processes. However, eye development, which also depends on Ras/MAPK signaling, is not affected in these mutants (*SI Appendix*, Fig. S7), which is consistent with a previous report on GOF Csw (the *Drosophila* ortholog of Shp2) mutations (31). Furthermore, because ectopic wing vein formation was sensitive to the weak mutation D44G and the other assays were not, this suggests that some cellular contexts are more sensitive to small perturbations in the Ras/MAPK pathway.

We believe that the ranking established in this study is informative and could be predictive of disease progression. For example, vertical transmission of RASopathy variants is rare, presumably occurring only in individuals carrying the weaker variants. Indeed, only E44G, a mutation revealed to be weak by our assay, was reported to be passed from parent to child (15). We also determined that our phenotypic ranking agrees with phenotypic severity reported in patients in certain studies by performing a pairwise comparison between phenotypes reported for different MEK1 mutations within a study. We performed this analysis by assigning a binary number, 0 or 1, for the absence or presence of reported aberrant phenotypes, respectively. Based on the literature, we find that an individual with F53S has more aberrant phenotypes than an individual with Y130C in the same study (*SI Appendix*, Table S5) (16). Similarly, L42F was found to be generally less severe than averaged data on two Y130C patients from the same study (*SI Appendix*, Table S5) (12). Although the patient data are not sufficient to perform statistics, these observations are largely consistent with our results. Hence, there are indeed indications of mutation-specific severity of human phenotypes. Clearly, this indicates a need for systematic mutation-based comparative analysis of human phenotypes.

It is important to know what features of hyperactivated signaling lead to different defects in the mutant backgrounds. One might expect some defects to emerge from the constitutive activity of RASopathy mutants where the pathway is active in the absence of upstream growth factors. In other cases, the defects could emerge from precocious activation or delayed deactivation of the pathway in tissues normally receiving transient Ras/MAPK activation. Although there have been a few attempts to answer related questions (48, 49), the assays used thus far have lacked quantitative spatiotemporal resolution. Therefore, our static measurements describing final outcomes, which allowed us to rank the mutations, should be complemented in the future by developing quantitative assays to study perturbations to signaling levels in a spatiotemporal manner.

Methods

Microinjection of Zebrafish Embryos. Microinjection of 500 pL (measured in mineral oil on a micrometer) of the RNA mixture (see *SI Appendix, SI Materials and Methods, RNA Synthesis for Microinjection*) at a concentration of ~110 pg/nL (i.e., 55 pg per embryo) was performed using the PV280 Pneumatic PicoPump (World Precision Instruments). A set of injected embryos was discarded if the injection bolus significantly decreased in size after the injection. Yolk injections were used for the aspect ratio assay, whereas one-cell injections were used for the heart size assay and for the drug treatments. Embryos and adults were raised and maintained at 28.5 °C. Embryos were acquired by pair mating of Tg(myl7:memGFP) (a gift from Fang Lin, University of Iowa, Iowa City, IA) (50) to PWT. Established zebrafish protocols were adhered to in accordance with the Princeton University Institutional Animal Care and Use Committee.

Generation of Transgenic Flies. Five mutations were introduced into Dsor1 (a gift from Alexey Veraksa, University of Massachusetts Boston, Boston) with site-directed mutagenesis using the Phusion enzyme (NEB) and verified by sequencing. WT and mutant versions were cloned into the transformation vector pTIGER (51) between the NheI and XbaI restriction sites. These constructs were integrated into the second chromosome using the ϕC31-based integration system (52) at the Attp site estimated to be at 25C6. Dsor1 expression is driven by the UAS promoter only in the presence of Gal4.

Zebrafish Phenotypes.

Aspect ratio. mRNA was injected at the one-cell stage, and the embryos were then sorted for the presence of phenol red after 2 h. At 11 hpf, the embryos were oriented on their side and imaged on the Leica M205 FA stereomicroscope. The major and minor axis of the yolk of the embryos were measured in ImageJ.

Lethality. After 48 hpf, an embryo was counted as being lethal if it was dead or if the embryo was grossly deformed, including severe cardiac edema and/or absence of a tail that would allow it to propel itself. The results in Fig. 1*C* were normalized to uninjected siblings with the following formula: normalized $\text{lethality}_{\text{Mutation}} = 1 - (1 - \text{lethality}_{\text{Mutation}}) / (1 - \text{lethality}_{\text{Uninjected siblings}})$.

Heart size. Embryos from a *Tg(myl7:memGFP)* and PWT cross were microinjected as described earlier and fixed with paraformaldehyde at 19.5 hpf in 4 °C overnight. After dechorionation and washes with PBS with Tween-20, the embryos were mounted in 1.5% low-melt agarose on the coverslip of a 35-mm dish with the heart positioned so as to be imaged on an upright Bruker Multi-Photon microscope. The *z* stacks of the hearts of multiple embryos injected

with a MEK variant as well as multiple uninjected siblings were taken. Using Imaris, these *z* stacks were oriented such that the viewing angle is perpendicular to the base of the heart cone and the resulting 2D image was exported to the TIF file format. This image was then opened in Imaris again, and the Surface tool was used to quantify the area that the heart cone occupied.

Fly Phenotypes.

Lethality. UAS-Dsor (WT and mutant) flies were crossed with MTD-Gal4, a maternal driver, for expression in the early embryo, and the eggs of the resulting females were collected. Analysis of embryonic lethality was performed at ∼40 h or later, after the embryos were laid by counting unhatched eggs.

Cuticle. Embryos were dechorionated after being aged for more than 24 h. Dechorionated embryos were shaken in methanol and heptane (1:1) and incubated overnight in a media containing lactic acid and Hoyer's media (1:1) at 65 °C. Embryos were imaged on a Nikon Eclipse Ni in darkfield.

Wing. Transgenic flies were crossed with Tubulin-Gal4, and the wings of the resulting progeny were imaged using a Leica M205 FA stereomicroscope. Wing metric is the average number of ectopic stereotypic wing veins (Fig. 4*A*).

Eye. Transgenic flies were crossed to GMR-Gal4, an eye-specific driver, and the resulting progeny were imaged using a Hitachi TM-1000 tabletop scanning electron microscope.

Statistical Analysis. For comparisons of three or more independent groups, the one-way analysis of variance (ANOVA) with Bonferroni correction and the Kruskal–Wallis test (nonparametric version of ANOVA) with the Bonferroni correction were used for statistical analysis. The data analysis was performed in MATLAB, where the anova1, kruskalwallis, and multcompare functions were used. For comparisons of two independent groups, Student's *t* test (two-sided, homoscedastic) was used, and data analysis was performed in Excel with the ttest function.

Additional experimental procedures are in *SI Appendix, SI Materials and Methods*. They include a description of fly stocks, RNA synthesis for microinjection, drug treatments, and protein blotting.

ACKNOWLEDGMENTS. We thank Cori Hasty, Phillip Johnson, Heather McAllister, and LAR staff for zebrafish care; Alexey Veraksa and Rony Seger for WT MEK constructs; Fang Lin for providing the *Tg(myl7:memGFP)* line; and Dr. Gary Laevsky and the Molecular Biology Confocal Microscopy Facility, which is a Nikon Center of Excellence, for microscopy support. We thank Elizabeth Goldsmith, Rony Seger, Alexey Veraksa, and Swathi Arur for helpful discussions. G.A.J. acknowledges support from National Science Foundation Graduate Research Fellowship Grant DGE 1148900. Y.G., K.Y., A.S.F., I.K., and S.Y.S. were supported by National Institutes of Health Grant R01 GM086537. C.A.B. and R.D.B. were supported by National Institutes of Health Grant R01 HD048584. T.S. is supported by National Institutes of Health Grant R01 GM077620.

1. Futran AS, Link AJ, Seger R, Shvartsman SY (2013) ERK as a model for systems biology of enzyme kinetics in cells. *Curr Biol* 23(21):R972–R979.
2. Jiang H, Grenley MO, Bravo M-J, Blumhagen RZ, Edgar BA (2011) EGFR/Ras/MAPK signaling mediates adult midgut epithelial homeostasis and regeneration in Drosophila. *Cell Stem Cell* 8(1):84–95.
3. Boulton TG, et al. (1990) An insulin-stimulated protein kinase similar to yeast kinases involved in cell cycle control. *Science* 249(4964):64–67.
4. Rauen KA (2013) The RASopathies. *Annu Rev Genomics Hum Genet* 14:355–369.
5. Jindal GA, Goyal Y, Burdine RD, Rauen KA, Shvartsman SY (2015) RASopathies: Unraveling mechanisms with animal models. *Dis Model Mech* 8(8):769–782.
6. Chen P-C, et al. (2014) Next-generation sequencing identifies rare variants associated with Noonan syndrome. *Proc Natl Acad Sci USA* 111(31):11473–11478.
7. Araki T, et al. (2004) Mouse model of Noonan syndrome reveals cell type- and gene dosage-dependent effects of Ptpn11 mutation. *Nat Med* 10(8):849–857.
8. Yu Z-H, et al. (2013) Structural and mechanistic insights into LEOPARD syndrome-associated SHP2 mutations. *J Biol Chem* 288(15):10472–10482.
9. Keilhack H, David FS, McGregor M, Cantley LC, Neel BG (2005) Diverse biochemical properties of Shp2 mutants. Implications for disease phenotypes. *J Biol Chem* 280(35):30984–30993.
10. Seger R, et al. (1992) Purification and characterization of mitogen-activated protein kinase activator(s) from epidermal growth factor-stimulated A431 cells. *J Biol Chem* 267(20):14373–14381.
11. Čizmárová M, et al. (2016) New mutations associated with Rasopathies in a central European population and genotype-phenotype correlations. *Ann Hum Genet* 80(1):50–62.
12. Dentici ML, et al. (2009) Spectrum of MEK1 and MEK2 gene mutations in cardio-facio-cutaneous syndrome and genotype-phenotype correlations. *Eur J Hum Genet* 17(6):733–740.
13. Nyström AM, et al. (2008) Noonan and cardio-facio-cutaneous syndromes: Two clinically and genetically overlapping disorders. *J Med Genet* 45(8):500–506.
14. Schulz AL, et al. (2008) Mutation and phenotypic spectrum in patients with cardio-facio-cutaneous and Costello syndrome. *Clin Genet* 73(1):62–70.
15. Nava C, et al. (2007) Cardio-facio-cutaneous and Noonan syndromes due to mutations in the RAS/MAPK signalling pathway: Genotype-phenotype relationships and overlap with Costello syndrome. *J Med Genet* 44(12):763–771.
16. Rodriguez-Viciana P, et al. (2006) Germline mutations in genes within the MAPK pathway cause cardio-facio-cutaneous syndrome. *Science* 311(5765):1287–1290.
17. Narumi Y, et al. (2007) Molecular and clinical characterization of cardio-facio-cutaneous (CFC) syndrome: Overlapping clinical manifestations with Costello syndrome. *Am J Med Genet A* 143A(8):799–807.
18. Gripp KW, et al. (2007) Further delineation of the phenotype resulting from BRAF or MEK1 germline mutations helps differentiate cardio-facio-cutaneous syndrome from Costello syndrome. *Am J Med Genet A* 143A(13):1472–1480.
19. Bromberg-White JL, Andersen NJ, Duesbery NS (2012) MEK genomics in development and disease. *Brief Funct Genomics* 11(4):300–310.
20. Kiel C, Serrano L (2014) Structure-energy-based predictions and network modelling of RASopathy and cancer missense mutations. *Mol Syst Biol* 10(5):727.
21. Scarpa A, et al. (2013) Molecular typing of lung adenocarcinoma on cytological samples using a multigene next generation sequencing panel. *PLoS One* 8(11):e80478.
22. Trunzer K, et al. (2013) Pharmacodynamic effects and mechanisms of resistance to vemurafenib in patients with metastatic melanoma. *J Clin Oncol* 31(14):1767–1774.
23. Armour CM, Allanson JE (2008) Further delineation of cardio-facio-cutaneous syndrome: Clinical features of 38 individuals with proven mutations. *J Med Genet* 45(4):249–254.
24. Allanson JE, et al. (2011) Cardio-facio-cutaneous syndrome: Does genotype predict phenotype? *Am J Med Genet C Semin Med Genet* 157C(2):129–135.
25. Roberts AE, Allanson JE, Tartaglia M, Gelb BD (2013) Noonan syndrome. *Lancet* 381(9863):333–342.
26. Cessans C, et al. (2016) Growth patterns of patients with Noonan syndrome: Correlation with age and genotype. *Eur J Endocrinol* 174(5):641–650.
27. Estep AL, Palmer C, McCormick F, Rauen KA (2007) Mutation analysis of BRAF, MEK1 and MEK2 in 15 ovarian cancer cell lines: Implications for therapy. *PLoS One* 2(12):e1279.
28. Nikolaev SI, et al. (2011) Exome sequencing identifies recurrent somatic MAP2K1 and MAP2K2 mutations in melanoma. *Nat Genet* 44(2):133–139.
29. Runtuwene V, et al. (2011) Noonan syndrome gain-of-function mutations in NRAS cause zebrafish gastrulation defects. *Dis Model Mech* 4(3):393–399.
30. Araki T, et al. (2009) Noonan syndrome cardiac defects are caused by PTPN11 acting in endocardium to enhance endocardial-mesenchymal transformation. *Proc Natl Acad Sci USA* 106(12):4736–4741.
31. Oishi K, et al. (2006) Transgenic Drosophila models of Noonan syndrome causing PTPN11 gain-of-function mutations. *Hum Mol Genet* 15(4):543–553.
32. Rauen KA, et al. (2010) Proceedings from the 2009 genetic syndromes of the Ras/MAPK pathway: From bedside to bench and back. *Am J Med Genet A* 152A(1):4–24.
33. Fürthauer M, Thisse C, Thisse B (1997) A role for FGF-8 in the dorsoventral patterning of the zebrafish gastrula. *Development* 124(21):4253–4264.
34. Fürthauer M, Van Celst J, Thisse C, Thisse B (2004) Fgf signalling controls the dorsoventral patterning of the zebrafish embryo. *Development* 131(12):2853–2864.
35. Jopling C, van Geemen D, den Hertog J (2007) Shp2 knockdown and Noonan/LEOPARD mutant Shp2-induced gastrulation defects. *PLoS Genet* 3(12):e225.
36. Anastasaki C, Estep AL, Marais R, Rauen KA, Patton EE (2009) Kinase-activating and kinase-impaired cardio-facio-cutaneous syndrome alleles have activity during zebrafish development and are sensitive to small molecule inhibitors. *Hum Mol Genet* 18(14):2543–2554.
37. Forbes SA, et al. (2015) COSMIC: Exploring the world's knowledge of somatic mutations in human cancer. *Nucleic Acids Res* 43(Database issue, D1):D805–D811.
38. Pierpont MEM, et al. (2014) Cardio-facio-cutaneous syndrome: Clinical features, diagnosis, and management guidelines. *Pediatrics* 134(4):e1149–e1162.
39. Bonetti M, et al. (2014) Noonan and LEOPARD syndrome Shp2 variants induce heart displacement defects in zebrafish. *Development* 141(9):1961–1970.
40. Molina G, et al. (2009) Zebrafish chemical screening reveals an inhibitor of Dusp6 that expands cardiac cell lineages. *Nat Chem Biol* 5(9):680–687.
41. Klingler M, Erdélyi M, Szabad J, Nüsslein-Volhard C (1988) Function of torso in determining the terminal anlagen of the Drosophila embryo. *Nature* 335(6187):275–277.
42. Baker NE, Rubin GM (1992) Ellipse mutations in the Drosophila homologue of the EGF receptor affect pattern formation, cell division, and cell death in eye imaginal discs. *Dev Biol* 150(2):381–396.
43. Testa ND, Dworkin I (2016) The sex-limited effects of mutations in the EGFR and TGF-β signaling pathways on shape and size sexual dimorphism and allometry in the Drosophila wing. *Dev Genes Evol* 226(3):159–171.
44. Diggs-Andrews KA, et al. (2014) Sex is a major determinant of neuronal dysfunction in neurofibromatosis type 1. *Ann Neurol* 75(2):309–316.
45. Inoue S, et al. (2014) New BRAF knockin mice provide a pathogenetic mechanism of developmental defects and a therapeutic approach in cardio-facio-cutaneous syndrome. *Hum Mol Genet* 23(24):6553–6566.
46. Anastasaki C, Rauen KA, Patton EE (2012) Continual low-level MEK inhibition ameliorates cardio-facio-cutaneous phenotypes in zebrafish. *Dis Model Mech* 5(4):546–552.
47. Jones S, et al. (2015) Personalized genomic analyses for cancer mutation discovery and interpretation. *Sci Transl Med* 7(283):283ra53.
48. Pagani MR, Oishi K, Gelb BD, Zhong Y (2009) The phosphatase SHP2 regulates the spacing effect for long-term memory induction. *Cell* 139(1):186–198.
49. Schuhmacher AJ, et al. (2008) A mouse model for Costello syndrome reveals an Ang II-mediated hypertensive condition. *J Clin Invest* 118(6):2169–2179.
50. Ye D, Xie H, Hu B, Lin F (2015) Endoderm convergence controls subduction of the myocardial precursors during heart-tube formation. *Development* 142(17):2928–2940.
51. Ferguson SB, Blundon MA, Klovstad MS, Schüpbach T (2012) Modulation of gurken translation by insulin and TOR signaling in Drosophila. *J Cell Sci* 125(Pt 6):1407–1419.
52. Bischof J, Maeda RK, Hediger M, Karch F, Basler K (2007) An optimized transgenesis system for Drosophila using germ-line-specific phiC31 integrases. *Proc Natl Acad Sci USA* 104(9):3312–3317.